Fe(III)-alginate and layered aluminum oxyhydroxide assisted hydro ceramsite composite for efficient removal of Se and As from high-concentration sulfate wastewater

Jingya Ren [a, *], Karen Leus [b], Rino Morent [b], Nathalie De Geyter [b], Pascal Van Der Voort [c], Gijs Du Laing[a]

[a] *Center for Advanced Process Technology and Urban Resource Recovery (CAPTURE), Department of Green Chemistry and Technology, Ghent University, Frieda Saeysstraat 1, 9052 Ghent, Belgium*

[b] *RUPT-Research Unit Plasma Technology, Department of Applied Physics, Ghent University, Sint-Pietersnieuwstraat 41 B4, 9000 Ghent, Belgium*

[c] *COMOC-Center for Ordered Materials, Organometallics and Catalysis, Department of Chemistry, Ghent University, Krijgslaan 281-S3, 9000 Ghent, Belgium*

*Corresponding authors.

E-mail addresses: Jingya.Ren@UGent.be; Tel: +32-456352421

ABSTRACT: In this work, hydro ceramsite (HC) was coated by layered aluminum oxyhydroxide (LAO) with the assistance of Iron(III)-alginate (IA) to obtain HC@LAO-IA. Iron(III)-alginate (IA) and layered aluminum oxyhydroxide (LAO) assist in the improvement of the adsorption capacity of hydro ceramsite (HC) for Se(IV), Se(VI), and As(V) via hydrogen bonding, electrostatic adsorption, and inner sphere complexation, respectively. HC@LAO-IA showed superior removal of Se(IV), Se(VI), and As(V) under simulated and actual environmental conditions in the presence of multiple competing anions (Cl^-, NO_3^-, CO_3^{2-}, PO_4^{3-} and SO_4^{2-}), particularly excelling in high-concentration sulfate wastewater, and also has a wide pH application range of 3-10. After four reuse cycles, HC@LAO-IA still exhibits satisfactory performance. Sand column experiments also demonstrated that HC@LAO-IA has excellent capabilities for the removal of Se(IV), Se(VI), and As(V) from real wastewater obtained from a metallurgical process plant. This work provides a promising, low-cost approach to remove Se and As from aqueous solutions and a new route for ceramsite recycling.

Keywords:

Hydro ceramsite, Layered aluminum oxyhydroxide, Selenate, Selenite, Arsenate

1. Introduction

Industrial activities, such as metal casting and coal mining, generate wastewater that contains toxic substances like selenium (Se) and arsenic (As), which can pose serious health risks to both aquatic animals and humans [1-4]. To mitigate these risks, industrial wastewater is often treated using chemical precipitation techniques, such as the addition of sulfate, sulfide or phosphate, to remove cationic heavy metals [5,6]. However, selenate and selenite, which are oxyanions with a chemical structure similar to sulfate and sulfite, are also present in wastewater. Sorption processes are an option to remove these oxyanions. Still, they can be difficult to remove from these wastewaters through sorption due to competition for sorption sites, especially when selenate concentrations are low compared to sulfate concentrations, or when arsenate concentrations are low compared to phosphate concentrations [7-9]. Therefore, the development of a novel efficient sorption strategy is crucial for arsenic and selenium removal especially from high-sulfate wastewater in order to meet the emission or environmental quality standards set by regulatory bodies such as the World Health Organization (WHO) and the United States Environmental Protection Agency (EPA).

Hydro ceramsite (HC), also known as hydroton clay balls or expanded clay, is a lightweight aggregate material used in concrete, plaster, and as a soil amendment in agriculture and construction. [10-12]. Recently, the development of HC-based agents for contaminant remediation has gained attention due to their low cost, high specific surface area and ion exchange properties [13-15]. Chen et al. [16] reported a porous ceramsite produced from multiple solid wastes to remove Pb (II) by bonding with Si—O or Al—O—Si—O embedded in the matrix of ceramsite. Niu et al. [17] prepared Fe_3O_4-modified ceramsite to convert Cr(VI) to Cr(III) and adsorb Cr(III) by electrostatic adsorption. Nevertheless, the application of these HC-based agents still

presents certain limitations, such as limited adsorption capacity, low selectivity, and high production cost. Other previous studies hardly focused on the selectivity of adsorbents for Se and As in high-concentration sulfate solutions or did not evaluate the developed adsorbents using real, non-simulated Se and As contaminated real wastewater, hampering the effective valorisation and commercialisation of developed adsorbents.

In this work, an HC-based agent named HC@LAO-IA for highly efficient removal of Se(IV), Se(VI) or As(V) from high-concentration sulfate wastewater was fabricated. The fabrication process and mechanism involved are illustrated in Fig. 1. Raw hydro ceramsite (HC) was washed with HCl solution to remove impurities from both its surface and interior. Afterwards, HC was immersed in a mixture of layered aluminum oxyhydroxide (LAO) and sodium alginate (SA) in solution, being uniformly coated onto the surface of HC to create HC@LAO-SA. Finally, the resulting HC@LAO-SA was crosslinked in $Fe(NO_3)_3$ solution to obtain HC@LAO-IA. The removal efficiencies of Se(IV), Se(VI) or As(V) in simulated and actual wastewater were investigated under various conditions, including the presence of competing ions. To reveal the removal mechanism, the interactions between HC@LAO-IA and Se(IV), Se(VI) or As(V) were studied. This work not only advances water treatment strategies for the removal of Se and As from high-concentration sulfate wastewater to meet stringent water quality thresholds but also presents a new direction for recycling ceramsite that has previously been used for other purposes.

2. Materials and methods

2.1 Synthesis of LAO

LAO, also named Ju-111 ($Al_3O_{2.5}(OH)_{3.5}Cl_{0.5}\cdot 0.9H_2O$), was synthesized by a simple hydrothermal method according to previous literature [18, 19]. Initially, 6.42 g

of CaO was dispersed in 165 mL of deionized water to form milky white suspension and stirred for 3 h. Subsequently, 27.54 g of $AlCl_3$ was added to the white suspension. All aforementioned reactions were carried out in a fume hood. After stirring the solution for 2 h, the solution gradually became transparent due to the hydrolysis reaction of $AlCl_3$. Then, the solution was transferred to five reaction vessels (50 mL) and heated at 180°C for 72 h. After cooling to room temperature, the solid product was washed 3 times with 70°C deionized water and dried at 100°C. Finally, the product was taken out and ground into powder using a mortar and pestle.

2.2 Fabrication of HC@LAO-IA

Raw HC spheres (100 g) were washed with 500 mL of HCl solution (3 mol/L) to eliminate impurities from both their surface and interior. The cleaned HCs (0.4 g) were soaked in SA (2g) and LAO (0.5-2.5g) hybrid suspension (50 mL) under continuous stirring (400 rpm) for 1 h at room temperature to obtain HC@LAO-SA. Eventually, the HC@LAO-SA was immersed in $Fe(NO_3)_3$ solution (0.09-0.25 mol/L) and stirred (350 rpm) for 1 h, leading to the formation of HC@LAO-IA through cross-linking between SA and Fe^{3+} [20, 21]. The resulting HC@LAO-IA was rinsed with deionized water 3 times to wash away residual Fe^{3+}. Prior to the production of HC@LAO-IA according to this procedure for use in subsequent adsorption experiments, various production conditions were tested. Results of this production process optimization experiment are presented in Fig. S1. The use of 0.4 g of HC, 50 mL of sodium alginate solution (20 g/L), 2 g of LAO and 0.17 mol/L of Fe(NO3)3 resulted in the highest Se(IV), Se(VI) and As(V) removal efficiency.

2.3 Batch adsorption experiments with HC@LAO-IA

In the adsorption experiments, 0.5 g of HC@LAO-IA was always added to 10 mL of Se(IV), Se(VI) or As(V) aqueous solutions. The resulting solutions were kept on a

shaker (200 rpm) for adsorption until equilibrium was achieved and subsequently separated using 0.45 μm membrane filters. Afterwards, the concentrations of Se(IV), Se(VI) or As(V) in solution were determined using an inductively coupled plasma-optical emission spectrometer (ICP-OES). Subsequently, the removal efficiencies of Se(IV), Se(VI) or As(V) and adsorption capacities of HC@LAO-IA (mg/g) were calculated according to equations (1) and (2):

$$RE\ (\%) = (C_0 - C_t)/C_0 \times 100\% \qquad (1)$$

$$Q_e = (C_0 - C_e)\frac{V}{m} \qquad (2)$$

where C_0 and C_t are the initial and residual concentrations (mg/L). C_e is the concentration at equilibrium (mg/L), and Q_e is the adsorption capacity of HC@LAO-IA at equilibrium. The time is measured in h, V represents the volume of solution in litres, and m is the weight of HC@LAO-IA in grams. All experiments were performed in duplicate.

2.4 Experiments to assess factors affecting Se(IV), Se(VI) or As(V) removal by HC@LAO-IA

To evaluate the removal efficiency and capacity of HC@LAO-IA for removal of Se(IV), Se(VI) or As(V) from low and high-concentrate solutions at different pH levels, HC@LAO-IA (0.5 g) was added to 10 mL of Se(IV), Se(VI) or As(V) (10 mg/L and 800 mg/L) aqueous solution at various pH conditions (2.0-11.0). pH values were adjusted with HCl (0.01 M to 1 M) and NaOH (0.01 M).

To investigate the influence of temperature and competing anions on Se(IV), Se(VI) or As(V) removal, 0.5 g of HC@LAO-IA was added to 10 mL of Se(IV), Se(VI) or As(V) (1 mg/L) aqueous solution with 500 mg/L of NaCl, Na_2CO_3, $NaNO_3$, Na_2SO_4 or Na_3PO_4, at different temperatures (10, 20, 30 and 40°C).

After 4 h, the HC@LAO-IA was taken out and the residual concentrations of

Se(IV), Se(VI) or As(V) were measured to calculate their removal efficiencies and adsorption capacities of HC@LAO-IA (mg/g) by equations (1) and (2). All experiments were performed in duplicate.

2.5 Adsorption kinetics and isotherms of HC@LAO-IA for Se(IV), Se(VI) or As(V)

To study the adsorption kinetics of HC@LAO-IA, 10 g of HC@LAO-IA was added to 250 mL of Se(IV), Se(VI) or As(V) (10 mg/L) at an initial pH value of 6.0. The resulting sample was placed on a shaker and 1 mL of the supernatant was aspirated at specific time points (from 0 min to 600 min). After that, all collected supernatants were diluted 10 times and quickly filtered through a 0.45 μm filter. Finally, the concentrations of Se and As were measured by ICP-OES. Pseudo-first-order and pseudo-second-order models were employed to fit the data and analyze the kinetics. Their linearized equations are given in Equations (3) and (4) [22, 23], respectively.

$$Ln(q_e-q_t)=Lnq_e-k_1t \qquad (3)$$

$$t/q_t=1/(k_2q_e^2)=t/q_e \qquad (4)$$

Where k_1 (min^{-1}) and k_2 ($g\cdot mg^{-1}\cdot min^{-1}$) are rate constants for pseudo-first-order and pseudo-second-order reactions, respectively. q_t and q_e (mg/g) represent adsorption capacities at time t (min) and equilibrium, respectively.

HC@LAO-IA was added to a series of solutions with different concentrations (from 200 mg/L to 1500 mg/L) of Se(IV), Se(VI) or As(V) at an initial pH of 6.0, and the resulting suspensions were shaken for 10 h. The solution concentrations before and after adsorption were determined by ICP-OES. The Se(IV), Se(VI) or As(V) adsorption isotherm of HC@LAO-IA was analyzed by fitting the data to the Langmuir (equation (5)) and Freundlich (equation (6)) model [22, 24].

$$C_e/q_e=C_e/Q_0+1/(Q_0b) \qquad (5)$$

$$q_e=K_FC_e^{1/n} \qquad (6)$$

where C_e (mg/L) represents equilibrium concentration; q_e (mg/g) is the adsorption capacity at equilibrium; Q_0 (mg/g) represents the maximum adsorption capacity; b (L/mg) is the Langmuir constant; K_F [mg/g (L/mg)$^{1/n}$] is the Freundlich constant; n is a constant that reflects the energetic heterogeneity.

2.6 Sand column experiment to study removal of Se(IV), Se(VI) or As(V) from metallurgical wastewater by HC@LAO-IA

Real industrial wastewater was collected from a metallurgical process plant. Firstly, the collected wastewater was filtered with filter paper (diameter 12.5 cm), and then the composition of the wastewater was analysed by ICP-OES and an Ion Chromatograph (IC). Silica sand (20-50 mesh, 50 g) was mixed with HC@LAO-IA (40 g) and placed in a glass column (length 20 cm, diameter 2.5 cm), and its top was sealed with glass wool (5 g) to prevent sand loss. The inclusion of silica sand in the column serves the purpose of enhancing column stability, maintaining a consistent flow profile, and preventing channeling. The prepared wastewater (800 mL) was pumped towards the reactor system at the speed of 2.00 mL/min, resulting in an empty bed contact time of 26.55 minutes. The effluents were collected in the outlet at specific time points (from 0 min to 540 min).

3. Results and discussion

3.1 Characterization of HC@LAO-IA

To elucidate the morphological and microstructural features of HC@LAO-IA**,** the HC@LAO-IA system was observed under SEM. Fig. 2a to 2b and Fig. 2d to 2e correspond to the surface and internal structure of HC, respectively, after hydrochloric acid treatment. The images reveal the presence of numerous pores within the HC ranging in size from 1 to 50 μm. Through BET analysis, the specific surface area of HC was found to be 2.28 m^2/g (Fig. S2). After HC was coated with LAO, LAO was firmly

embedded within the IA gel layer (Fig. 2c and 2f) and the surface pore structure was optimized. The specific surface area of HC@LAO-IA significantly increased to 11.32 cm^2/g (Fig. S2) and provided more Al-OH adsorption sites for Se(IV), Se(VI) and As(V) which was also confirmed by FTIR data presented in Fig. 2h. Simultaneously, the interconnected network of larger and smaller pores could facilitate the diffusion of Se(IV), Se(VI) and As(V) into the interior of HC, providing the possibility of contacting Se(IV), Se(VI) and As(V) with more amino groups on HC [25], further increasing the potential for Se(IV), Se(VI) and As(V) adsorption. In addition, the elemental mapping analysis (Fig. S3) suggested that the enhancement of Al signals on the outer surface of HC@LAO-IA, coupled with the concurrent reduction in the distinctive Si element signals inherent to HC, provides compelling evidence for the successful coating of HC by LAO-IA. In summary, this synergistic effect of structural modulation and surface optimization positions HC@LAO-IA as a highly efficient material for the adsorption of Se and As.

To investigate the composition and surface functional groups of the HC@LAO-IA composite material, XRD and FTIR analyses were performed. As shown in Fig. 2g, the XRD analysis revealed three distinct peaks at 24.1°, 26.7°, and 50.1°, corresponding to the mineral components of mullite calcium feldspar ($CaAl_2Si_2O_8$) and quartz (SiO_2) in HC [26, 27], as evidenced by the elemental mapping analysis in Fig. S3b and S3c. Besides, diffraction peaks at 11.1°, 21.1°, 24.8°, and 31.6°, corresponding to lattice planes of (010), (110), (120), and (200) of LAO [18, 19]. FTIR analysis of HC in Fig. 2h indicated the presence of $-NH_2$ groups and SiO_2 in HC at 3386 and 1045 cm^{-1}, corresponding to N–H and Si–O stretching vibrations [28, 29], respectively. Furthermore, the 890 cm^{-1} and 964 cm^{-1} peaks were identified as the Al-OH deformation mode vibration of LAO [19]. The FTIR analysis of HC@LAO-IA

demonstrated the presence of hydroxyl and amino groups (3147 to 3567 cm^{-1}), COO- stretching vibration of IA (1436 cm^{-1}) [30], Al-OH deformation mode vibration of LAO (896 cm^{-1} and 967 cm^{-1}), and Si–O stretching vibration of HC (1037 cm^{-1}). These results provide clear evidence of the successful synthesis of HC@LAO-IA and its surface functionalization with LAO, amino and carboxyl groups.

3.2 Adsorption by HC@LAO-IA as function of time and pH

The performance of HC@LAO-IA in terms of the removal of Se(VI), Se(IV), or As(V) from aqueous solutions was investigated. As illustrated in Fig. 3a, the efficiency of HC@LAO-IA for the removal of Se(VI), Se(IV), and As(V) increased with time, with the removal rates of Se(VI) and Se(IV) being nearly equivalent and reaching equilibrium after 3 hours. The removal rate of As(V) was slightly slower than that of Se(VI) and Se(IV), reaching equilibrium after 4 hours. After equilibrium was achieved, the removal efficiency for all three contaminants reached 99.9%.

Figure 3b-d depicted the adsorption performance of Se(IV), Se(VI), or As(V) at various pH values. In low-concentration solutions (10 mg/L) of these ions, their removal efficiency remained consistently high, reaching almost 99.9% over the pH range of 2-10. However, the removal efficiency of HC@LAO-IA for Se(IV), Se(VI), and As(V) dropped to around 85% at pH 11. This decrease could be due to the surplus hydroxide ions leading to the deprotonation of the functional groups on the surface of HC@LAO-IA, thereby impeding the adsorption of Se(IV), Se(VI), and As(V), while simultaneously damaging the coatings of IA and LAO [31]. The zeta potential measurements of HC@LAO-IA at various pH levels showed that the pH_{zpc} was around 6 (Fig. S4). The excellent acid-base buffering property of HC@LAO-IA maintains the equilibrium pH values in a narrow range under 6, leading to a positively charged surface favoring anion sorption [45]. This buffering effect, observed despite initial pH levels

exceeding 6, contributed to the efficacy of HC@LAO-IA in removing Se(IV), Se(VI), and As(V) across a pH range of 3-10.

In high-concentration solutions (800 mg/L) of Se(IV), Se(VI), or As(V), the adsorption capacity of HC@LAO-IA for these ions exhibited a pH-dependent trend. In the case of Se(IV), the removal capacity remained above 9.5 mg/g within the pH range of 2 to 11, with a slight decrease at pH 2. This trend could be attributed to the predominance of $HSeO_3^-$ and SeO_3^{2-} in this pH range, both carrying a net negative charge, facilitating their adsorption onto the positively charged surface of HC@LAO-IA [32]. The highest adsorption capacity was observed at pH 8, reaching 11.67 mg/g, possibly due to the formation of surface complexes between Se(IV) and functional groups of HC@LAO-IA at this pH [33].

The adsorption capacities of Se(VI) and As(V) exhibited a similar trend as pH varied. In the range of pH 2-6, the adsorption capacity increased initially and reached a maximum at pH 6, which was 10.88 mg/g for Se(VI) and 5.0 mg/g for As(V). From pH 6-11, the adsorption capacity of Se(VI) and As(V) showed a trend of initially decreasing, then increasing, and finally decreasing again. Therein, the increase of Se(VI) and As(V) adsorption capacities at pH 2 to 6 was probably because of the protonation of surface functional groups of HC@LAO-IA, leading to a more positive surface charge. At these pH values, $HSeO_4^{2-}$ and $H_2AsO_4^-$ forms are predominant Se and As species in solution, favoring increased Se(VI) and As(V) adsorption capacity [32, 34, 35]. In the pH increased from 6 to 11, Se(VI) and As(V) predominantly existed in SeO_4^{2-} and $HAsO_4^{2-}$ forms respectively [36-39]. In this pH range, the surface of HC@LAO-IA became more negatively charged due to the deprotonation of functional groups, which decreased the adsorption capacity for Se(VI) and As(V), especially in pH 11. Overall, the results suggested that HC@LAO-IA is a promising material for the effective removal of Se(IV),

Se(VI), or As(V) from contaminated wastewater, particularly in the pH range of 3-10.

3.3 Removal of Se(IV), Se(VI) or As(V) by HC@LAO-IA as affected by temperature and co-existing ions

To understand the performance of HC@LAO-IA in practical applications and to provide accurate parameters and conditions for its effective use, the influences of temperature (10, 20, 30 and 40 °C) and co-existing anions, including Cl^-, CO_3^{2-}, NO_3^-, SO_4^{2-} or PO_4^{3-}, on Se(IV), Se(VI) or As(V) removal by HC@LAO-IA were investigated. As shown in Fig. 4a and 4b, there was no significant difference in the removal efficiency of Se(IV), Se(VI) or As(V) by HC@LAO-IA at different temperatures, with removal rates all varying above 99.6%. This suggested that HC@LAO-IA exhibited good stability and consistency across various temperature conditions. At co-existing ion concentrations exceeding 500 times that of Se(IV), Se(VI), or As(V), the removal efficiency of these ions was unaffected by Cl^-, CO_3^{2-}, NO_3^-, or SO_4^{2-} (Fig. 4c-4d). However, when PO_4^{3-} concentration exceeded 500 times that of As(V), the removal efficiency of As(V) decreased to 81.3%, indicating competitive adsorption between PO_4^{3-} and As(V) [40, 41]. Overall, HC@LAO-IA demonstrated high stability and consistency in removing Se(IV), Se(VI), and As(V) under different temperatures and co-existing anion conditions, making it a promising option for practical applications in the treatment of water contaminated with these toxic substances.

The effectiveness of four materials (HC@LAO-CA, LAO@CA, LAO@IA and HC@LAO-IA) for the removal of Se(IV), Se(VI), or As(V) from high-concentration sulfate solutions was also examined. The synthesis methods for HC@LAO-CA, LAO@CA, and LAO@IA are given in Section S3. The results (Fig. 4e and 4f) clearly demonstrated that HC@LAO-IA exhibited the best removal efficiency for Se(IV), Se(VI), and As(V), especially for Se(VI), achieving a removal rate of 98.7%.

HC@LAO-CA, LAO@CA and LAO@IA showed comparatively lower removal rates of 54.7%, 24.5%, and 54.9%, respectively. The higher adsorption capacity of HC@LAO-IA for Se(VI) and As(V) in high-concentration sulfate solution was attributed to the presence of amine and carboxyl functional groups on IA and HC, which conferred better surface properties and stronger interactions with Se(VI) and As(V), compared to HC@LAO-CA, LAO@CA, and LAO@IA [31, 42]. In conclusion, the impact of high concentrations of SO_4^{2-} on Se(IV), Se(VI) and As(V) removal was negligible, demonstrating that HC@LAO-IA holds great promise for effectively removing Se(IV), Se(VI) and As(V) from sulfate-rich wastewater.

3.4 Adsorption isotherms and kinetics of HC@LAO-IA for Se(IV), Se(VI) and As(V) adsorption

The behavior of Se(IV), Se(VI) and As(V) adsorption on HC@LAO-IA was investigated by fitting the kinetic data to pseudo-first-order and pseudo-second-order models. The data could be better fitted by the pseudo-first-order kinetic model (Fig. 5a-5c), indicating that the adsorption process was predominantly chemical for Se(IV), Se(VI), and As(V), and the rate of adsorption was proportional to the concentration of the adsorbate within a certain concentration range. The IA coating on the surface of HC enhanced the stability and activity of LAO, leading to improved adsorption performance for the target pollutants. Notably, The k_2 values for Se(IV), Se(VI), and As(V) were determined to be 0.026, 0.027, and 0.009 g/(mg·min) (Table S1), respectively, with Se(IV) and Se(VI) exhibiting higher adsorption rates than As(V), consistent with the trends observed in Fig. 3a. Therefore, the adsorption of Se(IV), Se(VI), and As(V) on HC@LAO-IA was controlled by a pseudo-first-order kinetic model [43].

Furthermore, Langmuir and Freundlich isotherm models were utilized to further

examine the removal mechanism of Se(IV), Se(VI) and As(V). The fitting results (Fig. 6 and Table S2) showed that the adsorption isotherms of Se(IV), Se(VI), and As(V) were accurately described by the Freundlich model, with a higher R^2 value of 0.99 compared to that of the Langmuir model. Therefore, the adsorption of Se(IV), Se(VI), and As(V) on HC@LAO-IA was mainly heterogeneous [44]. The thermodynamic parameters for Se(IV), Se(VI) and As(V) adsorption on HC@LAO-IA, shown in Table S3, reveal negative ΔG^0 values, confirming the feasibility of Se and As adsorption on HC@LAO-IA [45]. The positive ΔS^0 values indicate the spontaneity of the adsorption process [46]. Additionally, compared to most sorbents listed in Table S4, such as Fe-based or Al-based materials, our results show excellent removal capacity of Se(IV), Se(VI), and As(V). Although iMOF exhibits better adsorption capacity than HC@LAO-IA, it faces challenges in upscaling, recycling/reuse and toxicity.

3.5. Performance of HC@LAO-IA for Se and As removal from real metallurgical process wastewater

To investigate the potential of treating real industrial wastewaters contaminated with selenium, arsenic, nitrate, phosphate, chloride, and sulfate ions, the concentrations of these ions, pH and redox potential of real wastewater collected at a metallurgical process plant were measured. The concentration of Se and As in this wastewater was 1.18 and 2.17 mg/L, respectively (Fig. 7a-7b). Therein, the pH and redox potential were determined to be 7.05 and 0.45V, respectively. $HAsO_4^{2-}$ (As(V)) is the predominant As form under these conditions [47]. It was worth noting that the wastewater contained high concentrations of chloride and sulfate ions, 4473 and 2577 mg/L, respectively. A column experiment was subsequently conducted to determine the efficacy of HC@LAO-IA in removing As and Se from the real wastewater. As shown in Fig 7c, after 6 hours, HC@LAO-IA demonstrated a remarkable adsorption rate of 98.9% for

As and a slightly reduced but still impressive rate of above 92% for Se. HC@LAO-IA also demonstrates superior adsorption performance for Se and As in the real metallurgical wastewater compared to goethite and schwertmannite (Fig. S7), and it outperforms other materials used in experiments investigating the influence of coexisting ions (Fig. 4e-4f), indicating its outstanding efficacy in removing Se and As from high-concentration sulfate real wastewater. The removal performance of HC@LAO-IA in real metallurgical wastewater after regeneration using sodium chloride decreased to 82% after the fourth cycle (Fig. S8). These findings highlight the potential of HC@LAO-IA for treating real industrial wastewater contaminated with toxic ions. However, other regeneration methods still need to be explored to further improve the reusability.

3.6. Characterization of HC@LAO-IA after adsorbing Se(IV), Se(VI) and As(V)

XRD measurements were also performed to investigate the interactions among Se(IV), Se(VI), As(V) and HC@LAO-IA. Figure 8a depicts the PXRD patterns of HC@LAO-IA both before and after Se(IV), Se(VI), or As(V) adsorption. Following adsorption, the peaks corresponding to the [010] plane were observed to shift significantly from 11.1° to 8.83°, 8.68°, and 8.67°, respectively, suggesting that larger Se(IV), Se(VI) or As(V) were able to enter the interlayer of LAO via ion exchange [18, 19]. Simultaneously, after treatment of simulated and real industrial wastewater, the concentrations of Fe leached from the adsorbent were all less than 0.4 mg/L (Table S5), indicating that HC@LAO-I possesses excellent stability, especially in real industrial wastewater.

In addition, FTIR spectroscopy was conducted to investigate the interaction between Se(IV), Se(VI) and As(V), and HC@LAO-IA. As shown in Fig 8b, after adsorption of Se(IV), Se(VI) or As(V) onto HC@LAO-IA, the smooth peak in the

3567-3147 cm^{-1} region shifted to 3455, 3305, and 3243 cm^{-1}, respectively. This is likely due to the hydrogen bonding formation between functional groups (-OH and $-NH_2$) and adsorbed oxygenated metal anions (SeO_3^{2-}, SeO_4^{2-} or AsO_4^{3-}), leading to a change in the peak position [48-50]. Similarly, the peak at 1436 cm^{-1} also blue-shifted to 1417, 1423, and 1425 cm^{-1}, which could be attributed to deprotonated -COOH groups on IA being replaced by Se(IV), Se(VI) or As(V) ions and adsorbed via electrostatic attraction [51]. Furthermore, the blueshift of the Al-OH deformation mode vibrational peak of LAO in HC@LAO-IA from 896 cm^{-1} to 889, 887, and 890 cm^{-1} may be due to the complexation between Al-OH and adsorbed oxygenated metal anions (SeO_3^{2-}, SeO_4^{2-}, or AsO_4^{3-}), after Cl- in LAO was exchanged with these anions through ion exchange adsorption [18, 19]. Similarly, in the Raman spectra of HC@LAO-IA/Se(IV), Se(VI) or As(V) (Fig.S5), three new bands are observed at 778 and 1069 cm^{-1} which can be attributed to ν1 symmetric stretching vibration of Se-O bond in SeO_3^{2-} and SeO_4^{2-}, and asymmetric stretching vibration of As-O bond in AsO_4^{3-}, respectively [19,52]. In conclusion, the surface structure of HC@LAO-IA was found to be altered upon Se or As adsorption, as evidenced by the FTIR and Raman analysis.

In order to characterize the surface chemistry of HC@LAO-IA before and after the adsorption of Se(IV), Se(VI) and As(V), XPS analysis was performed. Before adsorption, the XPS survey spectrum of HC@LAO-IA in Fig 8c showed signals for Al 2p, Si 2p and Fe 2p consistent with the LAO, HC and IA composition, as evidenced by the elemental mapping analysis in Fig. S3. In the high-resolution XPS spectra of the HC@LAO-IA, remarkable peaks corresponding to functional groups (-COOH and -OH on IA; $-NH_2$ on HC) were observed in Fig. S6a-c, including C=O (532.68 eV, 288.80 eV), C-O (286.40 eV), O-H (531.39 eV), C-N (287.40 eV), and $-NH_2$ (399.98 eV) [48]. Furthermore, characteristic peaks of Al-OH (74.4 eV) and Al-O (75.6 eV) on LAO were

also detected in the Al2p high-resolution spectra (Fig. S6d). Altogether, these findings provide compelling evidence for the successful immobilization of LAO and IA on HC.

After the adsorption of Se(IV), Se(VI) and As(V), the XPS survey spectrum in Fig. 8c showed the appearance of Se and As signals, indicating the successful adsorption of these species on the HC@LAO-IA inside and surface, as evidenced by the elemental mapping analysis data in Fig. S3e to S3f and Fig. S3k to S3l. High-resolution XPS spectra of Se 3d and As 3d regions were acquired to further confirm the adsorption. The Se 3d spectrum in Fig. 8d and 8e showed two peaks at 56.19 eV and 59.61eV, corresponding to the Se 3d3/2 and 3d5/2 spin-orbit doublets, respectively [53]. The chemical shifts to higher binding energy suggest that the Se species were in higher oxidation states, consistent with the expected Se(IV) and Se(VI) adsorption. The As 3d5/2 spectrum in Fig. 8f displayed a peak at 45.38 eV, consistent with As(V) species [54,55]. The observed decrease in the Cl signal in the XPS survey spectrum after adsorption suggests the displacement of Cl^- in LAO of HC@LAO-IA from the surface by Se(IV), Se(VI) and As(V) ions (Fig 8c). This displacement was attributed to the strong binding affinity of these oxyanions to the composite material surface. The shift of Al-OH and Al-O characteristic peaks towards higher binding energy, which symbolized LAO, also provided compelling evidence for the successful adsorption of some of the Se(IV), Se(VI) and As(V) ions. Additionally, the peaks of oxygen-containing groups (i.e., C=O, C-O and O-H groups) in both C 1s and O 1s spectra shifted to higher binding energies after adsorbing SeO_3^{2-}, SeO_4^{2-} and AsO_4^{3-}. These shifts may be primarily ascribed to the decrease of electron cloud density around oxygen atoms after bonding with the Se and As species via surface complexation interactions [56]. Notably, the peak of $–NH^+$ groups (407.78 eV) in the N 1s spectrum (Fig. S6g) appeared after adsorbing Se(IV), Se(VI) and As(V) ions, primarily ascribed

to the decreased electron cloud intensity of nitrogen atoms after binding with Se and As species via electrostatic interactions [57, 58]. Combining the results of the above adsorption experiments, it can be concluded that hydrogen bonding, electrostatic interactions and interlayer ion exchange in LAO may play a dominant role in the removal of Se(IV), Se(VI) and As(V).

3.7. Mechanisms involved in removal of Se(IV), Se(VI) and As(V) by HC@LAO-IA

Based on the above characterization analysis of HC@LAO-IA before and after Se(IV), Se(VI) or As(V) adsorption, it can be deduced that their removal occurs in three process steps: I. During the initial stage of sorption, Se(IV), Se(VI) or As(V) ions enter the LAO-IA layer and rapidly exchange with the free Cl^- ions present in the interlayer of LAO, and then fix onto the framework of LAO through inner-sphere complexation. II. Meanwhile, the presence of hydroxyl and deprotonated carboxyl groups on IA enables further adsorption of Se(IV), Se(VI), or As(V) through synergistic hydrogen bonding and electrostatic interactions. III. Upon entering the interior of HC, Se(IV), Se(VI), or As(V) can also be further adsorbed by the unique $–NH_2$ groups of HC via hydrogen bonding, thereby significantly enhancing the adsorption efficiency of HC@LAO-IA for these oxyanions.

Conclusion

A novel Fe(III)-alginate and layered aluminum oxyhydroxide assisted hydro ceramsite composite (HC@LAO-IA) was prepared after HC was loaded with LAO and IA. In the pH range of 3-10, HC@LAO-IA showed excellent efficiency for Se(IV), Se(VI), or As(V) removal from contaminated wastewater. Especially, HC@LAO-IA showed high potential for removing Se and As from simulated and actual wastewater contaminated with high concentrations of sulfate ions by inner sphere complexation,

hydrogen bonding and electrostatic adsorption. This work provides a promising approach to remediate Se(IV), Se(VI), or As(V) contaminated wastewater, especially in presence of high concentrations of sulfate ions, which may have a potential application prospect in environmental fields.

Credit Author Statement

Jingya Ren: Writing-Review & Editing, Supervision. Prof. Rino Morent, Prof. Nathalie De Geyter, and Dr. Karen Leus: Conducting X-ray photoelectron spectroscopy (XPS) and Scanning electron microscopy (SEM) experiments and analysis. Prof. Pascal Van Der Voort: Providing FTIR, XRD and Raman analysis. Gijs Du Laing: Formal analysis, Writing-Review & Editing, Supervision.

Declaration of Competing Interest

The authors declare that they have no known competing financial interests or personal relationships that could have appeared to influence the work reported in this paper.

Acknowledgements

We thank Joachim Nari for the guidance on experimental methods. J.Y.R. gratefully acknowledges the Chinese Scholarship Council (CSC) for financial support (202006500005).

References

[1] A. Deonarine, G.E. Schwartz, L.S. Ruhl, Environmental Impacts of Coal Combustion Residuals: Current Understanding and Future Perspectives, Environ. Sci. Technol. 57(5) (2023)1855-1869. https://doi.org/10.1021/acs.est.2c06094

[2] C. Guo, L. Hu, L. Jiang, H. Feng, B. Hu, T. Zeng, S. Song, H. Zhang, Toxic arsenic in marketed aquatic products from coastal cities in China: Occurrence, human dietary exposure risk, and coexposure risk with mercury and selenium, Environ. Pollut. 295 (2022) 118683. https://doi.org/10.1016/j.envpol.2021.118683

[3] O. Ouédraogo, M. Amyot, Mercury, arsenic and selenium concentrations in water and fish from sub-Saharan semi-arid freshwater reservoirs (Burkina Faso), Sci. Total Environ. 444 (2013) 243-254. https://doi.org/10.1016/j.scitotenv.2012.11.095

[4] M. ALSamman, S. Sotelo, J. Sánchez, B. Rivas, Arsenic oxidation and its subsequent removal from water: An overview, Sep. Purif. Technol. (2022) 123055. https://doi.org/10.1016/j.seppur.2022.123055

[5] J. Peng, Y. Song, P. Yuan, X. Cui, G. Qiu, The remediation of heavy metals contaminated sediment, J. Hazard. Mater. 161(2-3) (2009) 633-640. https://doi.org/10.1016/j.jhazmat.2008.04.061

[6] M. Matlock, B. Howerton, D. Atwood, Chemical precipitation of heavy metals from acid mine drainage, Water Res. 36(19) (2002) 4757-4764. https://doi.org/10.1016/S0043-1354(02)00149-5

[7] L. Pincus, H. Rudel, P. Petrović, S. Gupta, P. Westerhoff, C. Muhich, J. Zimmerman, Exploring the mechanisms of selectivity for environmentally significant oxo-anion

removal during water treatment: a review of common competing oxo-anions and tools for quantifying selective adsorption, Environ. Sci. Technol. 54(16) (2020) 9769-9790. https://doi.org/10.1021/acs.est.0c01666

[8] H. Chen, C. Shepsko, A. SenGupta, Use of a Novel Bio-Nano-IX Process to Remove SeO_4^{2-} or Se (VI) from Contaminated Water in the Presence of Competing Sulfate (SO_4^{2-}), ACS ES&T Water, 1(8) (2021) 1859-1867. https://doi.org/10.1021/acsestwater.1c00126

[9] L. Weerasundara, Y. Ok, J. Bundschuh, Selective removal of arsenic in water: A critical review, Environ. Pollut. 268 (2021) 115668. https://doi.org/10.1016/j.envpol.2020.115668

[10] E. Roces, M. Muñiz-Menéndez, J. González-Galindo, J. Estaire, Lightweight expanded clay aggregate properties based on laboratory testing, Constr. Build Mater. 313 (2021) 125486. https://doi.org/10.1016/j.conbuildmat.2021.125486

[11] A. Rashad, Lightweight expanded clay aggregate as a building material–An overview, Constr. Build Mater. 170 (2018) 757-775. https://doi.org/10.1016/j.conbuildmat.2018.03.009

[12] Q. Shao, Y. Zhang, Z. Liu, L. Long, Z. Liu, Y. Chen, X. Hu, M. Lu, L. Huang, Phosphorus and nitrogen recovery from wastewater by ceramsite: Adsorption mechanism, plant cultivation and sustainability analysis, Sci. Total Environ. 805 (2022) 150288. https://doi.org/10.1016/j.scitotenv.2021.150288

[13] J. Wang, Y. Zhao, P. Zhang, L. Yang, G. Xi, Adsorption characteristics of a novel ceramsite for heavy metal removal from stormwater runoff, Chin. J. Chem. Eng. 26(1)

(2018) 96-103. https://doi.org/10.1016/j.cjche.2017.04.011

[14] J. Qi, Z. Zhu, Z. Chen, X. Wang, Y. Zhang, H. Chen, Synthesis, Characterization and application of dewatered municipal sludge-based creamsite and its phosphorus adsorption characteristics, J. Clean. Prod. 391 (2023) 136216. https://doi.org/10.1016/j.jclepro.2023.136216

[15] S. Jiang, P. Rao, H. Huan, L. Liu, Y. Luo, W. Wang, X. Du, H. Yang, J. Tian, Performance of a ceramsite-enhanced gravity-driven ceramic membrane (GDCM) for simultaneous manganese ion and ammonia removal, J. Clean. Prod. (2023) 136082. https://doi.org/10.1016/j.jclepro.2023.136082

[16] Y. Chen, J. Shi, H. Ron, X. Zhou, F. Chen, X. Li, T. Wang, H. Hou, Adsorption mechanism of lead ions on porous ceramsite prepared by co-combustion ash of sewage sludge and biomass, Sci. Total Environ. 702 (2020) 135017. https://doi.org/10.1016/j.scitotenv.2019.135017

[17] J. Niu, P. Ding, X. Jia, G. Hu, Z. Li, Study of the properties and mechanism of deep reduction and efficient adsorption of Cr (VI) by low-cost Fe_3O_4-modified ceramsite, Sci. Total Environ. 688 (2019) 994-1004. https://doi.org/10.1016/j.scitotenv.2019.06.333

[18] P. Bai, Z. Dong, S. Wang, X. Wang, Y. Li, Y. Wang, Y. Ma, W. Yan, X. Zou, J. Yu, A layered cationic aluminum oxyhydroxide as a highly efficient and selective trap for heavy metal oxyanions, Angew. Chem. Int. Ed. Engl. 59(44) (2020) 19539-19544. https://doi.org/10.1002/anie.202005878

[19] H. Cai, H. Bao, X. Zhang, L. Lei, C. Xiao, Highly efficient sorption of selenate

and selenite onto a cationic layered single hydroxide via anion exchange and inner-sphere complexation, Chem. Eng. J. 420 (2021) 129726. https://doi.org/10.1016/j.cej.2021.129726

[20] J. Wu, H. Zhen, F. Zhang, R. Zeng, B. Xin, Iron-carbon composite from carbonization of iron-crosslinked sodium alginate for Cr (VI) removal, Chem. Eng. J. 362 (2019) 21-29. https://doi.org/10.1016/j.cej.2019.01.009

[21] H. Vu, A. Dwivedi, T. Le, S. Seo, E. Kim, Y. Chang, Magnetite graphene oxide encapsulated in alginate beads for enhanced adsorption of Cr (VI) and As (V) from aqueous solutions: Role of crosslinking metal cations in pH control, Chem. Eng. J. 307 (2017) 220-229. https://doi.org/10.1016/j.cej.2016.08.058

[22] R. Ezzati, Derivation of pseudo-first-order, pseudo-second-order and modified pseudo-first-order rate equations from Langmuir and Freundlich isotherms for adsorption, Chem. Eng. J. 392 (2020) 123705. https://doi.org/10.1016/j.cej.2019.123705

[23] C. Yan, Z. Cheng, Y. Tia, F. Qiu, H. Chang, S. Li, Y. Cai, X. Quan, Adsorption of Ni (II) on detoxified chromite ore processing residue using citrus peel as reductive mediator: Adsorbent preparation, kinetics, isotherm, and thermodynamics analysis, J. Clean. Prod. 315 (2021) 128209. https://doi.org/10.1016/j.jclepro.2021.128209

[24] V. Ramya, D. Murugan, C. Lajapathirai, S. Meenatchisundaram, S. Arumugam, A composite adsorbent of superparamagnetic nanoparticles with sludge biomass derived activated carbon for the removal of chromium (VI), J. Clean. Prod. 366 (2022) 132853. https://doi.org/10.1016/j.jclepro.2022.132853

[25] M. Chaudhary, S. Rawat, A. Maiti, Defluoridation by bare nanoadsorbents,

nanocomposites, and nanoadsorbent loaded mixed matrix membranes, Sep. Purif. Rev. 52(2) (2023) 135-153. https://doi.org/10.1080/15422119.2022.2045610

[26] C. Ou, J. Wang, W. Yang, Y. Bao, Z. Liao, J. Shi, J. Qin, Removal of ammonia nitrogen and phosphorus by porous slow-release Ca^{2+} ceramsite prepared from industrial solid wastes, Sep. Purif. Technol. 304 (2023) 122366. https://doi.org/10.1016/j.seppur.2022.122366

[27] N. Li, B. Lai, L. Ding, J. Li, C. Liu, L. Wu, Synchronous algae and phosphorus removal by Ceramsite@ Fe_2O_3 (FC) via taking the algae as crystal nuclei of hydroxylapatite, Chem. Eng. J. 426 (2021) 130748. https://doi.org/10.1016/j.cej.2021.130748

[28] Y. Chen, N. Wang, S. An, C. Cai, J. Peng, M. Xie, J. Peng, X. Song, Synthesis of novel hierarchical porous zeolitization ceramsite from industrial waste as efficient adsorbent for separation of ammonia nitrogen, Sep. Purif. Technol. 297 (2022) 121418. https://doi.org/10.1016/j.seppur.2022.121418

[29] Y. Shi, W. Guo, Y. Jia, C. Xue, Y. Qiu, Q. Zhao, D. Wang, Preparation of non-sintered lightweight aggregate ceramsite based on red mud-carbide slag-fly ash: Strength and curing method optimization, J. Clean. Prod. 372 (2022) 133788. https://doi.org/10.1016/j.jclepro.2022.133788

[30] B. Swamy, Y. Yun, In vitro release of metformin from iron (III) cross-linked alginate–carboxymethyl cellulose hydrogel beads, Int. J. Biol. Macromol. 77 (2015) 114-119. https://doi.org/10.1016/j.ijbiomac.2015.03.019

[31] D. Roquero, A. Othman, A. Melman, E. Katz, Iron (III)-cross-linked alginate

hydrogels: A critical review, Adv. Mater. 3(4) (2022) 1849-1873. https://doi.org/10.1039/D1MA00959A

[32] J. Tong, J. Yang, L. Zhang, T. Liu, C. Peng, X. Ni, T. Dong, P. Mocilac, K. Shi, X. Hou, Efficient removal of Se-79 from highly acidic solution using SiO_2 particles functionalised with iron hydroxide, Chem. Eng. J. 446 (2022) 137387. https://doi.org/10.1016/j.cej.2022.137387

[33] L. Zhang, S. Jiang, Y. Guan, Efficient removal of selenate in water by cationic poly (allyltrimethylammonium) grafted chitosan and biochar composite, Environ. Res. 194 (2021) 110667. https://doi.org/10.1016/j.envres.2020.110667

[34] K. Kalaitzidou, A. Nikoletopoulos, N. Tsiftsakis, F. Pinakidou, M. Mitrakas, Adsorption of Se (IV) and Se (VI) species by iron oxy-hydroxides: Effect of positive surface charge density, Sci. Total Environ. 687 (2019) 1197-1206. https://doi.org/10.1016/j.scitotenv.2019.06.174

[35] Y. Wu, C. Guan, N. Griswold, L. Hou, X. Fang, A. Hu, Z. Hu, C. Yu, Zero-valent iron-based technologies for removal of heavy metal (loid) s and organic pollutants from the aquatic environment: Recent advances and perspectives, J. Clean. Prod. 277 (2020) 123478. https://doi.org/10.1016/j.jclepro.2020.123478

[36] M. Li, C. Wang, M. OConnell , C. Chan, Carbon nanosphere adsorbents for removal of arsenate and selenate from water, Environ. Sci. Nano, 2(3) (2015) 245-250. https://doi.org/10.1039/C4EN00204K

[37] C. Tabelin, R. Sasaki, T. Igarashi, I. Park, S. Tamoto, T. Arima, M. Ito, N. Hiroyoshi, Simultaneous leaching of arsenite, arsenate, selenite and selenate, and their migration

in tunnel-excavated sedimentary rocks: II. Kinetic and reactive transport modeling, Chemosphere, 188 (2017) 444-454. https://doi.org/10.1016/j.chemosphere.2017.08.088

[38] J. Yamani, A. Lounsbury, J. Zimmerman, Towards a selective adsorbent for arsenate and selenite in the presence of phosphate: Assessment of adsorption efficiency, mechanism, and binary separation factors of the chitosan-copper complex, Water Res. 88 (2016) 889-896. https://doi.org/10.1016/j.watres.2015.11.017

[39] L. Camacho, R. Parra, S. Deng, Arsenic removal from groundwater by MnO_2^- modified natural clinoptilolite zeolite: Effects of pH and initial feed concentration, J. Hazard. Mater. 189(1-2) (2011) 286-293. https://doi.org/10.1016/j.jhazmat.2011.02.035

[40] Y. Han, J. Park, Y. Min, D. Lim, Competitive adsorption between phosphate and arsenic in soil containing iron sulfide: XAS experiment and DFT calculation approaches, Chem. Eng. J. 397 (2020) 125426. https://doi.org/10.1016/j.cej.2020.125426

[41] X. Li, L. Yan, W. Zhong, M. Kersten, C. Jing, Competitive arsenate and phosphate adsorption on α-FeOOH, LaOOH, and nano-TiO_2: Two-dimensional correlation spectroscopy study, J. Hazard. Mater. 414 (2021) 125512. https://doi.org/10.1016/j.jhazmat.2021.125512

[42] S. Anita, F. Ardiati, M. Oktaviani, F. Sari, O. Nurhayat, K. Ramadhan, D. Yanto, Immobilization of laccase from Trametes hirsuta EDN 082 in light expanded clay aggregate for decolorization of Remazol Brilliant Blue R dye, Bioresour. Technol. Rep. 12 (2020) 100602. https://doi.org/10.1016/j.biteb.2020.100602

[43] O. Kazak, A. Tor, In situ preparation of magnetic hydrochar by co-hydrothermal treatment of waste vinasse with red mud and its adsorption property for Pb (II) in

aqueous solution, J. Hazard Mater. 393 (2020) 122391. https://doi.org/10.1016/j.jhazmat.2020.122391

[44] I. Mohammed, A. Jawad, A. Abdulhameed, M. Mastuli, Physicochemical modification of chitosan with fly ash and tripolyphosphate for removal of reactive red 120 dye: statistical optimization and mechanism study, Int. J. Biol. Macromol. 161 (2020) 503-513. https://doi.org/10.1016/j.ijbiomac.2020.06.069

[45] N. Jain, A. Maiti, Fe-Mn-Al metal oxides/oxyhydroxides as As (III) oxidant under visible light and adsorption of total arsenic in the groundwater environment, Sep. Purif. Technol. 302 (2022) 122170. https://doi.org/10.1016/j.seppur.2022.122170

[46] N. Jain, A. Maiti, Arsenite Oxidation and Arsenic Adsorption Strategy Using Developed Material from Laterite and Ferromanganese Slag: Electron Paramagnetic Resonance Spectroscopy Analysis, Ind. Eng. Chem. Res. 62(38) (2023) 15600-15612. https://doi.org/10.1021/acs.iecr.3c01377

[47] M. Charykova, V. Krivovichev, Mineral systems and thermodynamic stability of arsenic minerals in the environment, In Processes and Phenomena on the Boundary Between Biogenic and Abiogenic Nature, (2020) 259-276. https://doi.org/10.1007/978-3-030-21614-6_15

[48] F. Ahmadpoor, S. Shojaosadati, S. Mousavi, Magnetic silica coated iron carbide/alginate beads: synthesis and application for adsorption of Cu (II) from aqueous solutions, Int. J. Biol. Macromol. 128 (2019) 941-947. https://doi.org/10.1016/j.ijbiomac.2019.01.173

[49] Y. Zhang, X. Xu, C. Yue, L. Song, Y. Lv, F. Liu, A. Li, Insight into the efficient co-

removal of Cr (VI) and Cr (III) by positively charged UiO-66-NH_2 decorated ultrafiltration membrane, Chem. Eng. J. 404 (2021) 126546. https://doi.org/10.1016/j.cej.2020.126546

[50] Z. Lu, J. Yu, H. Zeng, Q. Liu, Polyamine-modified magnetic graphene oxide nanocomposite for enhanced selenium removal, Sep. Purif. Technol. 183 (2017) 249-257. https://doi.org/10.1016/j.seppur.2017.04.010

[51] J. Wu, R. Zeng, In situ preparation of stabilized iron sulfide nanoparticle-impregnated alginate composite for selenite remediation, Environ. Sci. Technol. 52(11) (2018) 6487-6496. https://doi.org/10.1021/acs.est.7b05861

[52] Y. Penke, A.Yadav, I. Malik, A.Tyagi, J. Ramkumar, K. Kar, Insights of arsenic (III/V) adsorption and electrosorption mechanism onto multi synergistic (redox-photoelectrochemical-ROS) aluminum substituted copper ferrite impregnated rGO, Chemosphere, 267 (2021) 129246. https://doi.org/10.1016/j.chemosphere.2020.129246

[53] D. Han, B. Batchelor, A. Abdel-Wahab, XPS analysis of sorption of selenium (IV) and selenium (VI) to mackinawite (FeS), Environ. Prog. Sustain. Energy, 32(1) (2013) 84-93. https://doi.org/10.1002/ep.10609

[54] H. Viltres, O. Odio, L. Lartundo-Rojas, E. Reguera, Degradation study of arsenic oxides under XPS measurements, Appl. Surf. Sci. 511 (2020) 145606. https://doi.org/10.1016/j.apsusc.2020.145606

[55] N. Jain, A. Maiti, Arsenic adsorbent derived from the ferromanganese slag, Environ. Sci. Pollut. Res. 28 (2021) 3230-3242. https://doi.org/10.1007/s11356-020-10745-9

[56] A. Hassan, A. Abdel-Mohsen, H. Elhadidy, Adsorption of arsenic by activated carbon, calcium alginate and their composite beads, Int. J. Biol. Macromol. 68 (2014) 125-130. https://doi.org/10.1016/j.ijbiomac.2014.04.006

[57] B. Rathi, P. Kumar, A review on sources, Identification and treatment strategies for the removal of toxic Arsenic from water system, J. Hazard Mater. 418 (2021) 126299. https://doi.org/10.1016/j.jhazmat.2021.12629

[58] P. Fan, Y. Sun, B. Zhou, X. Guan, Coupled effect of sulfidation and ferrous dosing on selenate removal by zerovalent iron under aerobic conditions, Environ. Sci. Technol. 53(24) (2019) 14577-14585. https://doi.org/10.1021/acs.est.9b04956

Figure captions:

Figure 1. Schematic illustration of the fabrication process of HC@LAO-IA

Figure 2. SEM images of (a, b) HC surface and (d, e) HC interior, and (c, f) LAO-IA; FTIR spectra (g) and XRD patterns (h) of HC@LAO-IA.

Figure 3. (a) Influence of time on removal efficiency of Se(IV), Se(VI) and As(V) by HC@LAO-IA at 25ºC (initial concentration 10 mg/L); (b,c,d) Influence of pH on removal efficiency and adsorption capacity of Se(IV) (b), Se(VI) (c) and As(V) (d) by HC@LAO-IA at 25°C (initial concentrations 10 mg/L and 800 mg/L).

Figure 4. Influence of (a and b) temperature at pH 6 on Se(IV), Se(VI), and As(V) removal efficiency of HC@LAO-IA; (c) Effect of co-existing anions on Se(IV), Se(VI), and As(V) (d) removal efficiency of HC@LAO-IA. The effectiveness of four materials in removing (e) Se(IV), Se(VI), or (f) As(V) from high-concentration sulfate solutions (initial concentrations: 1 mg/L of Se(IV), Se(VI), or As(V) and 500 mg/L of SO_4^{2-}).

Figure 5. Adsorption kinetics plots for adsorption of (a) Se(IV), (b) Se(VI) and (c) As(V) onto HC@LAO-IA, respectively (C_0 of Se(IV), Se(VI) and As(V): 10 mg/L each, pH 6.0, 25 °C, 200 rpm).

Figure 6. Equilibrium isotherms plots for adsorption of (a) Se(IV), (b) Se(VI), and (c) As(V) onto HC@LAO-IA (C_0 of Se(IV), Se(VI) and As(V): 200 mg/L-1500 mg/L each, pH 6.0, 25 °C, 200 rpm).

Figure 7. (a-b) The concentration of various anions in actual metallurgical process wastewater; (c) Column experiment of HC@LAO-IA in actual metallurgical process wastewater.

Figure 8. (a) XRD patterns, (b) FTIR spectra, (c) full-range XPS spectra and (d-f) Se3d/As3d XPS spectra of HC@LAO-IA before and after Se(IV), Se(VI), or As(V) adsorption.

682 **Figures**

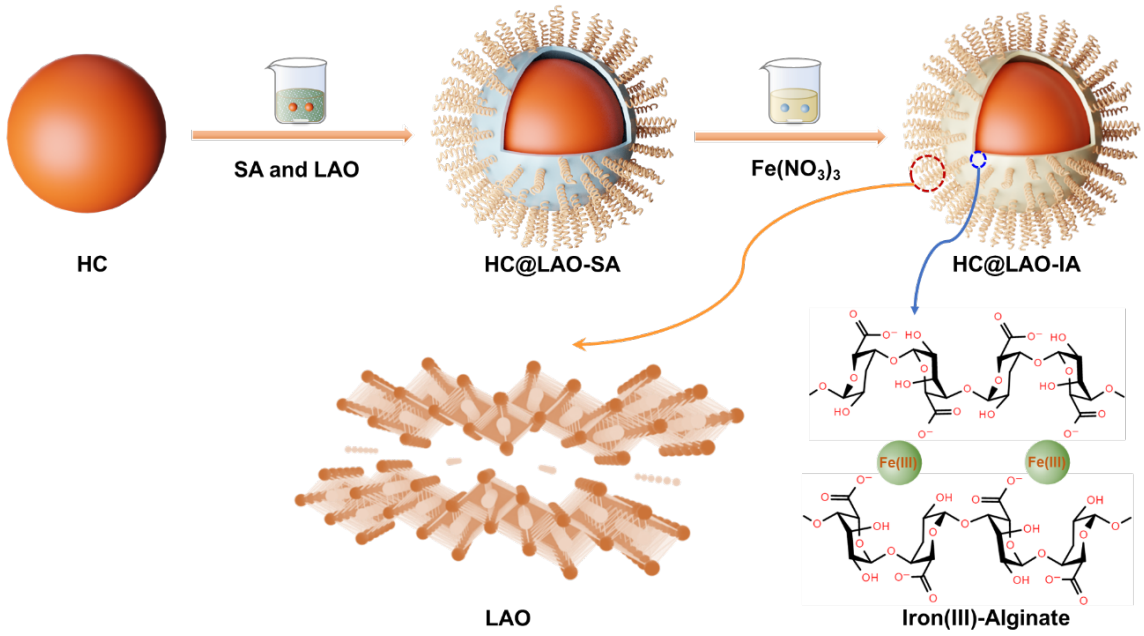

683

684 Figure 1

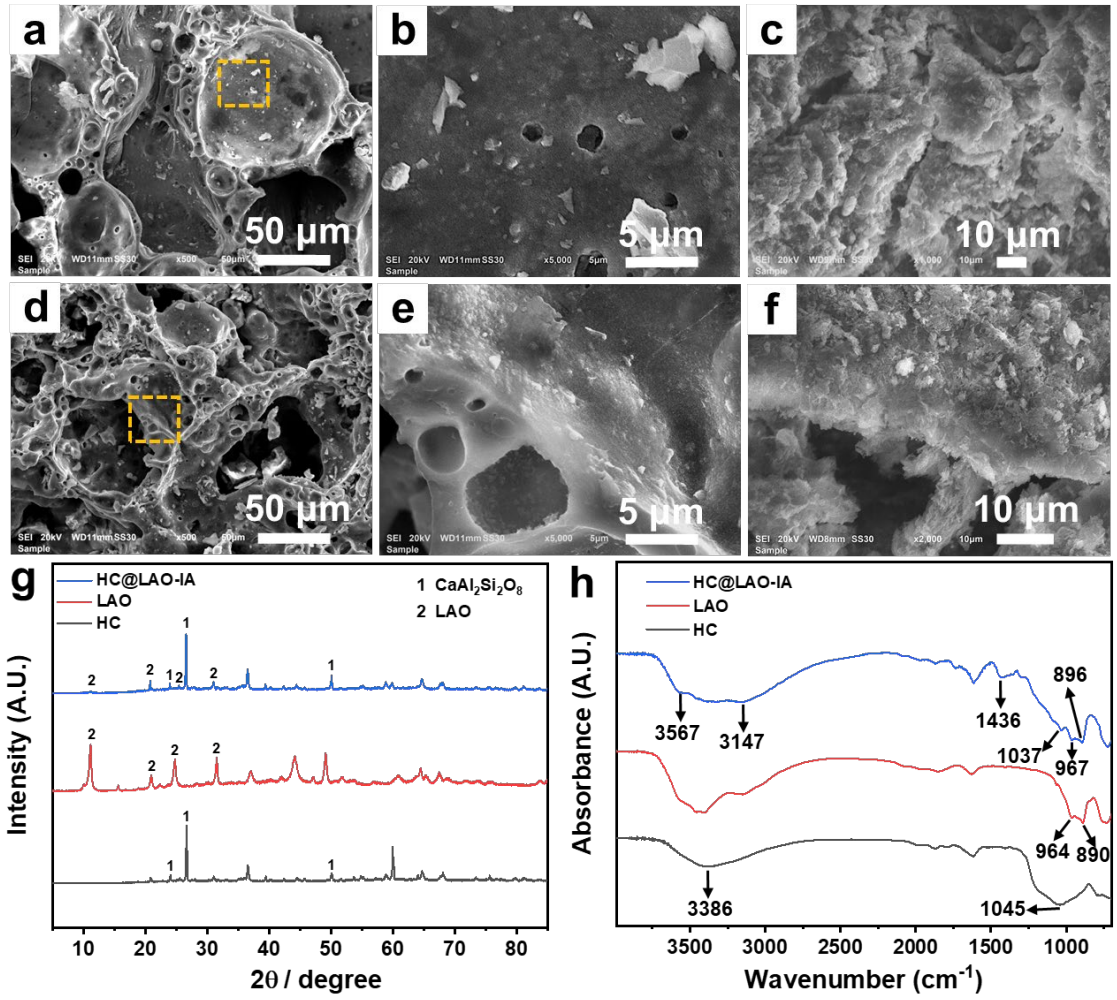
a
50 μm
b
5 μm
c
10 μm
d
50 μm
e
5 μm
f
10 μm
g
HC@LAO-IA
LAO
HC
1 CaAl2Si2O8
2 LAO
Intensity (A.U.)
2θ / degree
h
HC@LAO-IA
LAO
HC
Absorbance (A.U.)
3567
3147
1436
896
1037
967
964
890
3386
1045
Wavenumber (cm-1)

Figure 2

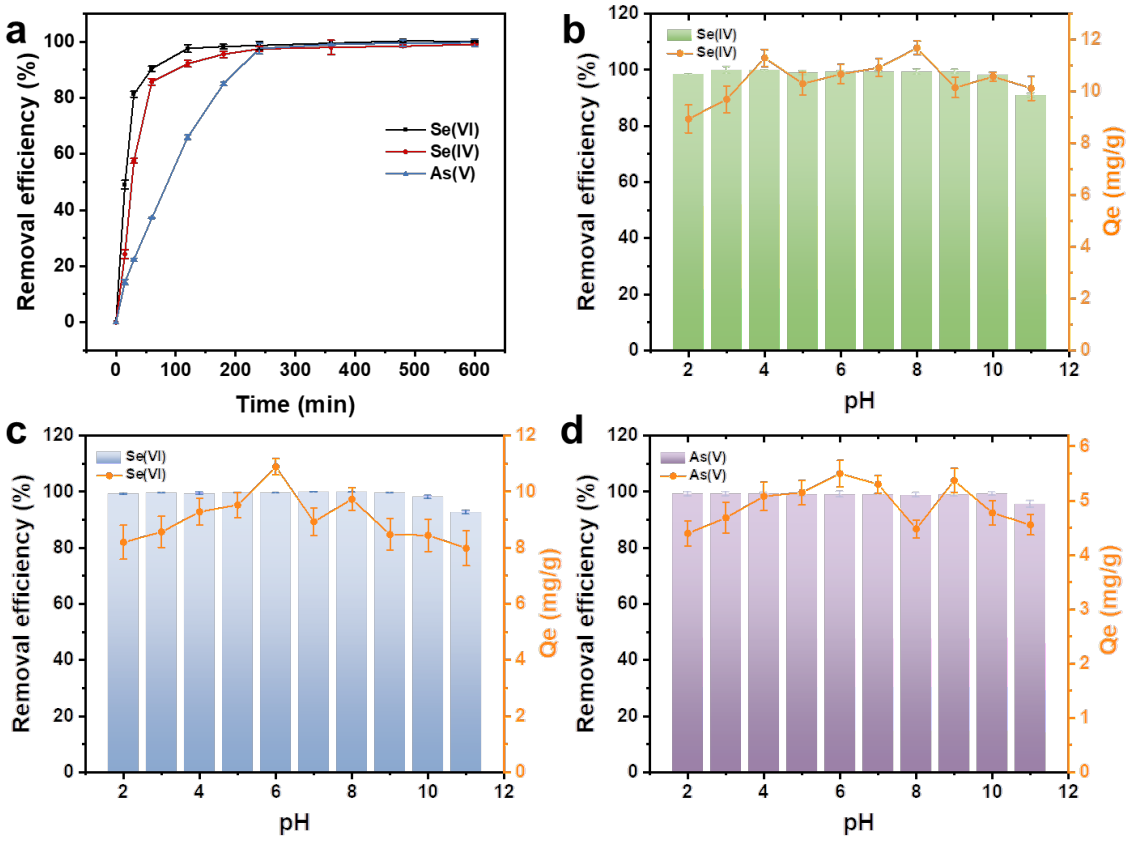
a
Removal efficiency (%)
Time (min)
Se(VI)
Se(IV)
As(V)
b
Se(IV)
Se(IV)
Removal efficiency (%)
Qe (mg/g)
pH
c
Se(VI)
Se(VI)
Removal efficiency (%)
Qe (mg/g)
pH
d
As(V)
As(V)
Removal efficiency (%)
Qe (mg/g)
pH

Figure 3

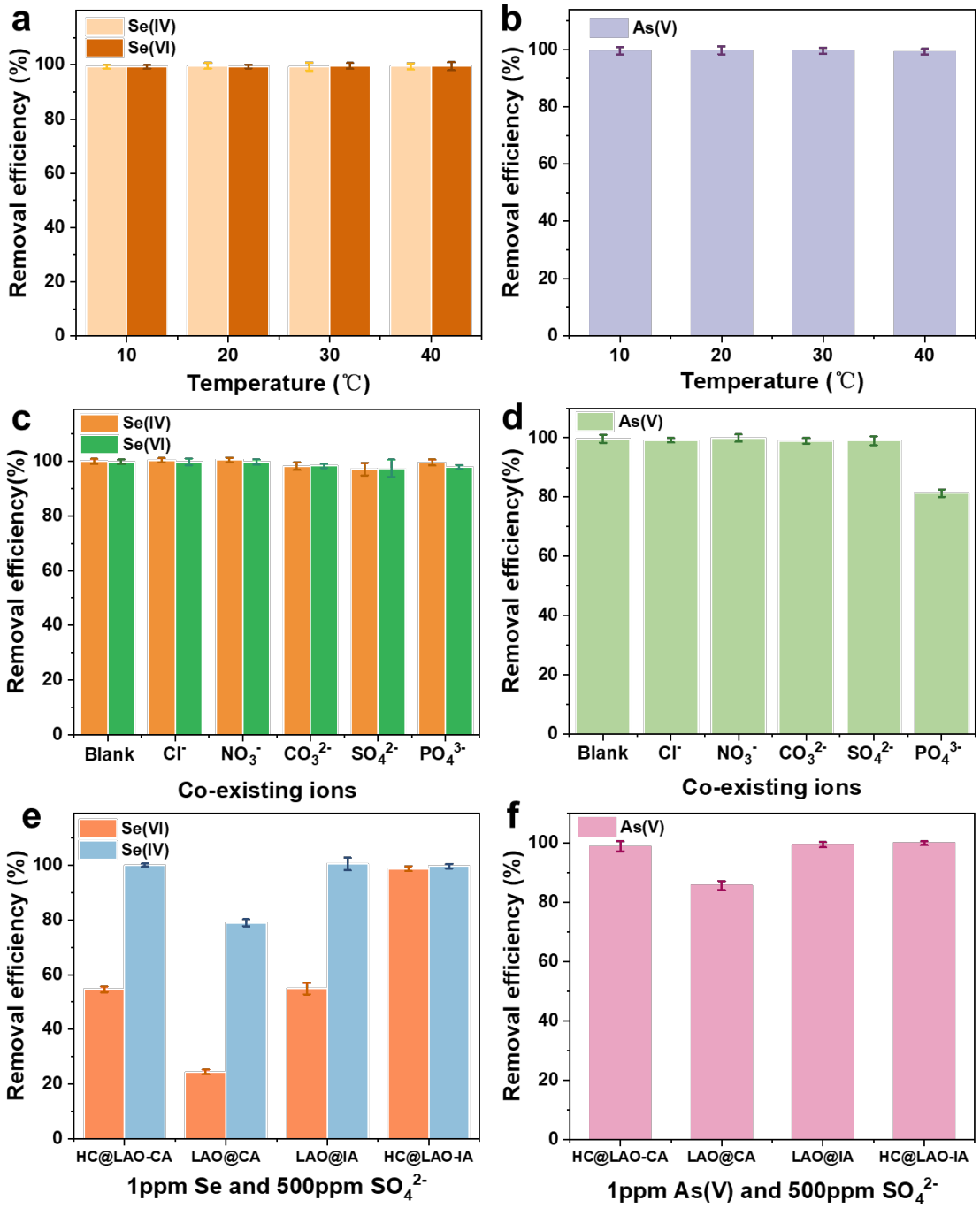
a
Se(IV)
Se(VI)
Removal efficiency (%)
Temperature (℃)
b
As(V)
Removal efficiency (%)
Temperature (℃)
c
Se(IV)
Se(VI)
Removal efficiency(%)
Blank
Cl-
NO3-
CO32-
SO42-
PO43-
Co-existing ions
d
As(V)
Removal efficiency(%)
Co-existing ions
e
Se(VI)
Se(IV)
Removal efficiency (%)
HC@LAO-CA
LAO@CA
LAO@IA
HC@LAO-IA
1ppm Se and 500ppm SO42-
f
As(V)
Removal efficiency (%)
1ppm As(V) and 500ppm SO42-

Figure 4

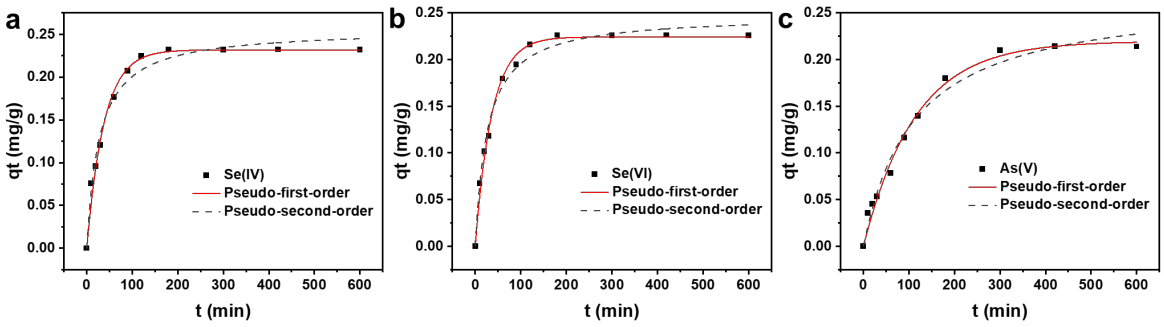
a
b
c
qt (mg/g)
t (min)
Se(IV)
Se(VI)
As(V)
Pseudo-first-order
Pseudo-second-order

Figure 5

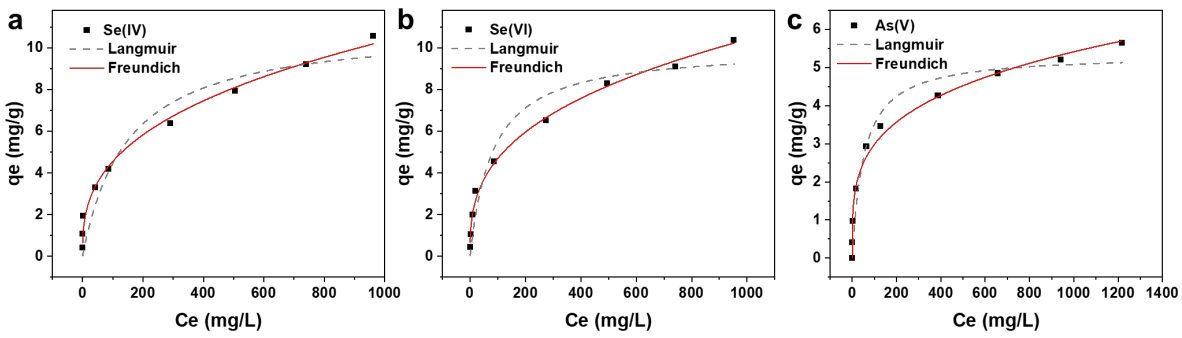
a
Se(IV)
Langmuir
Freundich
qe (mg/g)
Ce (mg/L)
b
Se(VI)
Langmuir
Freundich
qe (mg/g)
Ce (mg/L)
c
As(V)
Langmuir
Freundich
qe (mg/g)
Ce (mg/L)

Figure 6

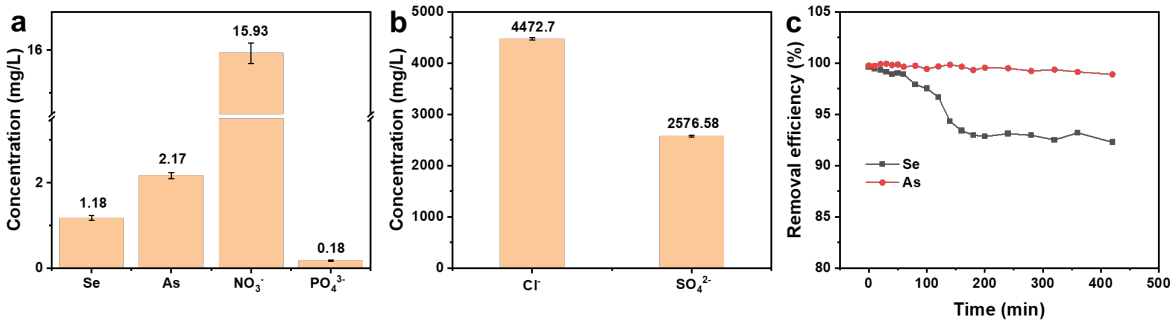
a
Concentration (mg/L)
16
2
0
1.18
2.17
15.93
0.18
Se
As
NO3-
PO43-
b
Concentration (mg/L)
5000
4000
3000
2000
1000
0
4472.7
2576.58
Cl-
SO42-
c
Removal efficiency (%)
105
100
95
90
85
80
Se
As
0
100
200
300
400
500
Time (min)

Figure 7

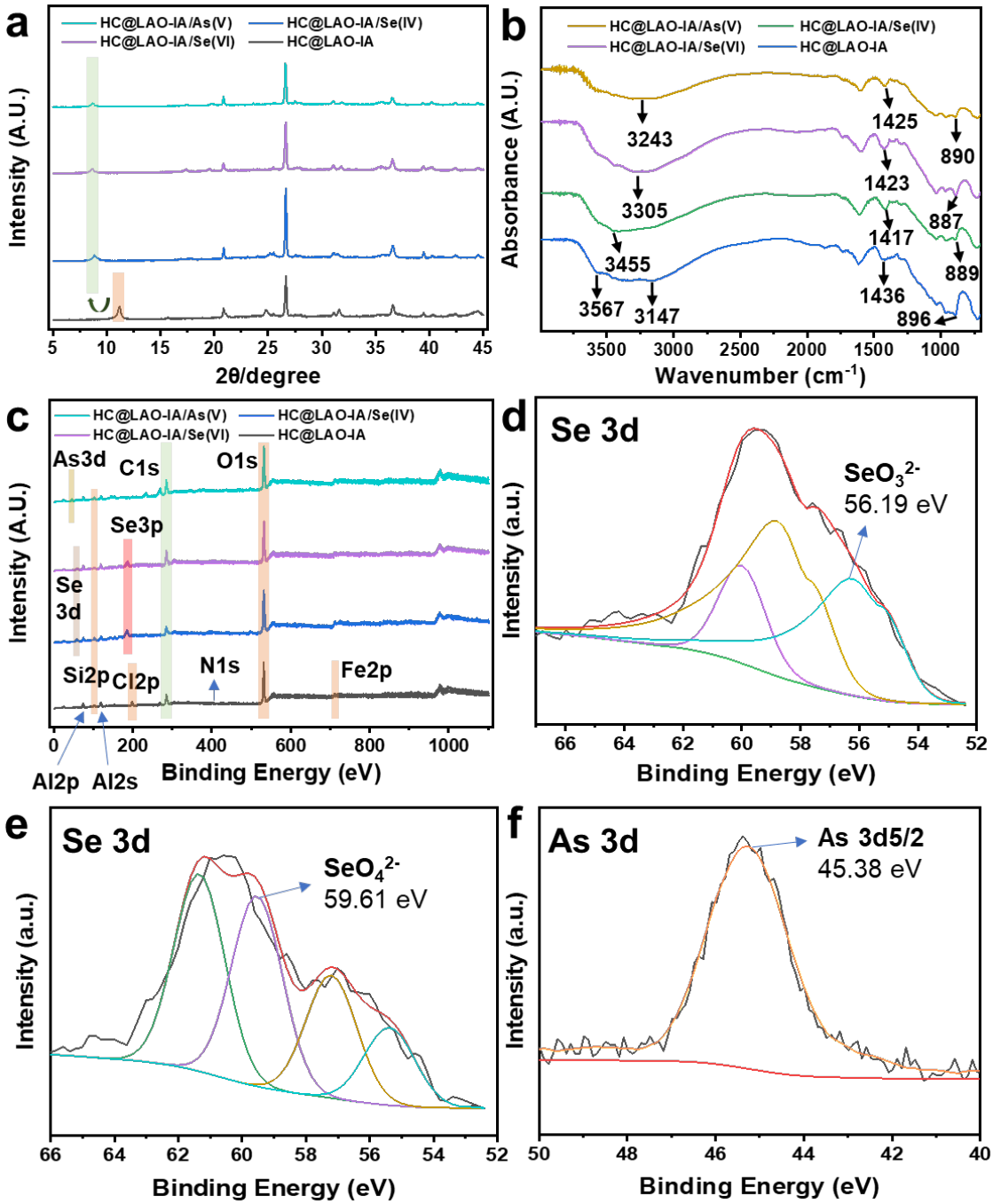
a
HC@LAO-IA/As(V)
HC@LAO-IA/Se(IV)
HC@LAO-IA/Se(VI)
HC@LAO-IA
Intensity (A.U.)
2θ/degree
b
Absorbance (A.U.)
3243
3305
3455
3567
3147
1425
1423
1417
1436
890
887
889
896
Wavenumber (cm-1)
c
As3d
C1s
O1s
Se3p
Se 3d
Si2p
Cl2p
N1s
Fe2p
Al2p
Al2s
Binding Energy (eV)
d
Se 3d
SeO3 2-
56.19 eV
Intensity (a.u.)
Binding Energy (eV)
e
Se 3d
SeO4 2-
59.61 eV
Intensity (a.u.)
Binding Energy (eV)
f
As 3d
As 3d5/2
45.38 eV
Intensity (a.u.)
Binding Energy (eV)

Figure 8